2018

# Laser-sculpted hybrid photonic magnetometer with nanoscale magnetostrictive interaction

Allsop, T



10.1016/j.sna.2017.12.021
Sensors and Actuators A: Physical
Elsevier BV

Sensors and Actuators A 269 (2018) 545–555

Contents lists available at ScienceDirect

Sensors and Actuators A: Physical

journal homepage: www.elsevier.com/locate/sna

# Laser-sculpted hybrid photonic magnetometer with nanoscale magnetostrictive interaction

Thomas Allsop [a], Graham B. Lee [a], Changle Wang [a,*], Ronald Neal [b], Kyriacos Kalli [c], Philip Culverhouse [b], David J. Webb [a]

[a] Aston Institute of Photonic Technologies, Aston University, Aston Triangle, Birmingham, B4 7ET, UK
[b] School of Computing, Electronics and Mathematics, Faculty of Science and Technology, University of Plymouth, Plymouth, PL4 8AA, UK
[c] Nanophotonics Research Laboratory, Department of Electrical Engineering, Computer Engineering and Informatics, Cyprus University of Technology, 31 Archbishop Kyprianos, Lemessos 3036, Cyprus

ARTICLE INFO

*Article history:*
Received 25 April 2017
Received in revised form
23 November 2017
Accepted 11 December 2017
Available online 12 December 2017

*Keywords:*
Magnetostrictive material
Long period gratings
Optical sensing
Magnetic sensors

ABSTRACT

We present a new photonic magnetic sensor that can yield information on the spatial angle of rotation of the sensor within a given static magnetic field that based upon an optical fiber platform that has a wavelength-encoded output and a demonstrated sensitivity of 543 pm/mT. This optical fiber magnetic field sensor combines a conventional, UV-laser inscribed long period grating (LPG) with a magnetostrictive material Terfenol-D that coats and fills 50-μm micro-slots running adjacent and parallel to the fiber central axis. The micro-slots are produced using a femtosecond laser and selective chemical etching. A detection limit for a static magnetic field strength of ±50 μT is realized in low strength DC magnetic field (below 0.4 mT), this performance approaches the Earth's magnetic field strength and thus, once optimized, has potential for navigation applications. Our method addresses the major drawback of conventional sensors, namely their inadequate sensitivity to low strength, static magnetic fields and their inability to provide information about the orientation and magnitude.



## 1. Introduction

There is significant interest in detecting and monitoring electromagnetic fields (EMF) generated in a number of industries, for applications related to process control, electric field monitoring in medicine, ballistic control, electromagnetic compatibility measurements and the potential health risks associated with environmental exposure to overhead power cables [1,2]. Other potential applications have been explored such as current sensors, load cells, accelerometers, proximity sensors, non-contact torque sensors and magnetometers [3–6]. Specifically, magnetometers are widely used for navigation and in geophysical research involving measuring the Earth's magnetic field (25–65 μT) [7]. There is interest in using optical fiber sensors that stems from their many advantages; they have high reliability, with low maintenance requirements, immunity to high voltage and electromagnetic interference, light weight, compactness and the capability to function in many hostile environments where conventional sensors would possibly fail. Orthodox EMF measurement systems are based on an active metallic probe that can perturb the EMF being sensed. Moreover, this sensing approach is susceptible and vulnerable to electromagnetic noise [8]. There are other types of magnetic field sensors that are based upon on different magnetic effects. These types of sensors include, one, magnetoresistance sensors [9] which are generally sensitive to a magnetic field applied in a single direction but they can have issues with angular cross-field errors and possible saturation response with small field strengths. Two, magnetoimpedance which are used to measure alternating magnetic field and not static magnetic fields, furthermore some of the materials used produce stripe domains [10] that can affect the performance of the sensor and complex designs are been used with varying success [11]. Three, anisotropic magnetoresistance but typically don't have good sensitivity to measure low strength DC magnetic fields [12]. Again, the aforementioned three effects are measured electrically which have the same vulnerable as the conventional EMF detection systems. In contrast, the sensing of EMF with fiber optic sensors demonstrates great benefits compared with electronic devices; these beneficial attributes include excellent galvanic insulation, high sensitivity and very large bandwidth.

There are a myriad of fiber optic sensing platforms for detecting magnetic fields that utilize the magnetostrictive effect in specific materials. These ferromagnetic materials produce a strain in the

* Corresponding author.
*E-mail address:* wangc15@aston.ac.uk (C. Wang).

https://doi.org/10.1016/j.sna.2017.12.021

direction of the magnetic field, thus generating a longitudinal strain within the optical fiber itself [3,13–15]. All of these fiber optic sensors have several operating deficiencies, principally, their poor performance leads to an inability to detect low static magnetic field strengths. Researchers have used an array of magnetostrictive fiber optic to yield directional information and magnitude of the applied magnetic field [16,17] but operated in high strength magnetic fields and poor sensitivity to low strength fields. Furthermore, from the literature there is no reported sensitivity dependence on orientation within a magnetic field for single magnetostrictive fiber optic sensor. There are other types of optic fiber sensor that yield magnetic field orientation, such as, those based upon the interaction of guides modes or surface plasmons with magnetic fluids [18,19], again these sensors have a poor performance in detecting low static magnetic fields.

We present here a new optical fiber magnetic field sensor, comprising a conventional UV-laser inscribed long period grating (LPG) adjacent to 50-μm long micro-slots that are located parallel to the fiber central axis. The micro-slots were delineated using a femtosecond laser and revealed by a hydrofluoric acid etching process [20]. The fiber was coated, and the micro-slots filled, with Terfenol-D, a magnetostrictive material, by using sputtering technology. This new optical fiber magnetic field sensor has a very high maximum spectral sensitivity to B-field ($\Delta\lambda/\Delta B$ of −543 pm/mT), an optimum resolution of ±50 μT for magnetic field strengths below 0.4 mT and a resolution of ±100 μT above 1 mT.

The LPG attenuation band response to B-fields exhibits both red and blue spectral shifts; these change in wavelength is dependent upon the spatial orientation of the sensor to the magnetic field. The wavelength shifts produced by the fiber devices are a combination of geometrical shape birefringence, created by the micro-slots/Terfenol-D monoliths, and stress induced birefringence produced by the Terfenol-D in response to a DC magnetic field (expansion or contraction), along with changes to the polarization state of the illuminating light produced by rotation of the fiber.

The investigation is to create a single optical fiber magnetic field sensor to that as a marked improvement in performance over the existing fiber optic sensors with regards to sensitivity, limit of detection and to have the intrinsic ability to differentiate various directions of the DC magnetic fields. Furthermore, to achieve an increase in performance such that the earth's magnetic field can be detect with such a fiber optic magnetometer offers various applications already mentioned above. Whilst our device is not a true vectorial fiber optic magnetic field sensor, nevertheless it offers information on the orientation and magnitude of the sensor within a DC magnetic field. We note that the Faraday effect can be exploited for such purposes [21], but the Verdet constant is very low in glass, thus limiting the range of potential applications to those where large field strengths are present, for example as a magnetic field sensor for use in high power, electrical machinery. Furthermore, the resolution of this type of fiber optic magnetometer in low strength DC magnetic field is ±50 μT which is approaching the values of the earth's magnetic field (25–65 μT).

## 2. Magnetic sensor modelling

An LPG structure was chosen over a fiber Bragg grating [22], based on earlier experimental investigations that showed the latter provided lower sensitivity [3]. The LPG's phase matching condition has many dependent parameters, in particular, the cladding effective index, and the Terfenol-D monoliths in our structures, can regionally change this value in the presence of a magnetic field. Moreover, the transmission spectra of LPGs written into asymmetric fibers (in this case caused by the femtosecond laser microslots) can yield information on the orientation of any bend experienced by the fiber [23].

The period of the LPG was chosen so that the attenuation bands coincided with the bandwidth of the available light sources. This involved calculating the propagation constants for the core and cladding modes [24] (the optical fiber is commercial grade SMF-28 from Dow Corning Inc.) over a range of wavelengths and producing phase matching curves, leading to a suitable period of 430 μm. For this period, there are several attenuation bands present from 1300 nm to 1700 nm (Fig. 1 a). The second step was to determine the spatial position of the Terfenol-D monoliths, with reference to the core of the optical fiber, which yields the greatest perturbation on an individual cladding mode, and thus higher, geometrical shape birefringence. This was estimated by using a Finite Element Method software package (Comsol) to inspect the radial E-field distributions of the cladding modes and looking at the largest overlap between the monolith and the E-field at a radial distance from the core sufficient to yield asymmetric spectral behavior. In the presence of magnetic field the monoliths would produce detectable, asymmetric strains dependent on the direction of any local magnetic field. This radial distance was estimated to be approximately 28 μm (Fig. 1b). The monolith length of 50 μm and width of 10 μm was chosen from previous work [25]. Increasing the size of the micro-slots and their number causes an increase in mechanical fragility [25], so this size represents something of a compromise. The final step was to estimate the strain-inducing effect of the Terfenol-D in a magnetic field and thereby determine the change in the effective refractive index of the cladding glass by using the strain-optic coefficient of SMF-28 (0.24) [24], as a first approximation. Furthermore, if the fiber with the sensor is rotated, the authors realize this rotation will generate additional torsional strain (via the strain-optic coefficients [26]; $p_{4,4}$) inducing elliptical birefringence and change the polarization. This rotational action in an asymmetric fiber (possessing elliptical birefringence), when rotated clockwise or anticlockwise, results in increasing or decreasing birefringence [27]. Hence the Terfenol-D monolith, with the correct orientations to the magnetic field, can produce stress to either add or reduce the local birefringence, resulting in red or blue wavelength shifts of the LPGs attenuation bands. The calculation of the induced strain was undertaken in several steps. Using information provided by the manufacturer of the Terfenol-D [3], and assuming an ideal mechanical coupling between the monoliths and the glass, the magnetic field induced radial variation in the effective index was included in a FEM model of the machined fiber incorporating the Terfenol-D. An example of radial variation in strain across the optical fiber is shown in Fig. 1c, and an example of the perturbed E-field of a cladding mode in the perpendicular plane of travel is shown in Fig. 1d.

Using the FEM model for different strength magnetic fields and including the spatial orientation of the B-field lines, the model allowed us to calculate variations in the propagation constants associated with magnetic field strength and orientation. This approximation assumes that the propagation constants already incorporate the shape birefringence, and the Terfenol-D stress-induced birefringence, caused by the radial generated strain by the Terfenol-D monoliths in the presents of static magnetic field, can be calculated using the approach given in REF 28, which includes the assumption that stress contribution wavelength dependence $P_\lambda$ is attributed to chromatic dispersion of the stress optical coefficient given in REF 28, thus the stress birefringence $\Delta n_{stress}$ and polarization dispersion $P_\lambda$:

$$\Delta n_{stress} = PS_{max} \; and \; P_\lambda = \frac{S_{max}}{c}\left(P - \lambda\frac{dP}{d\lambda}\right)$$

Where $P$ is the stress optical coefficient, $S_{max}$ is the maximum difference in the radial stress/strain produced by the Terfenol-D

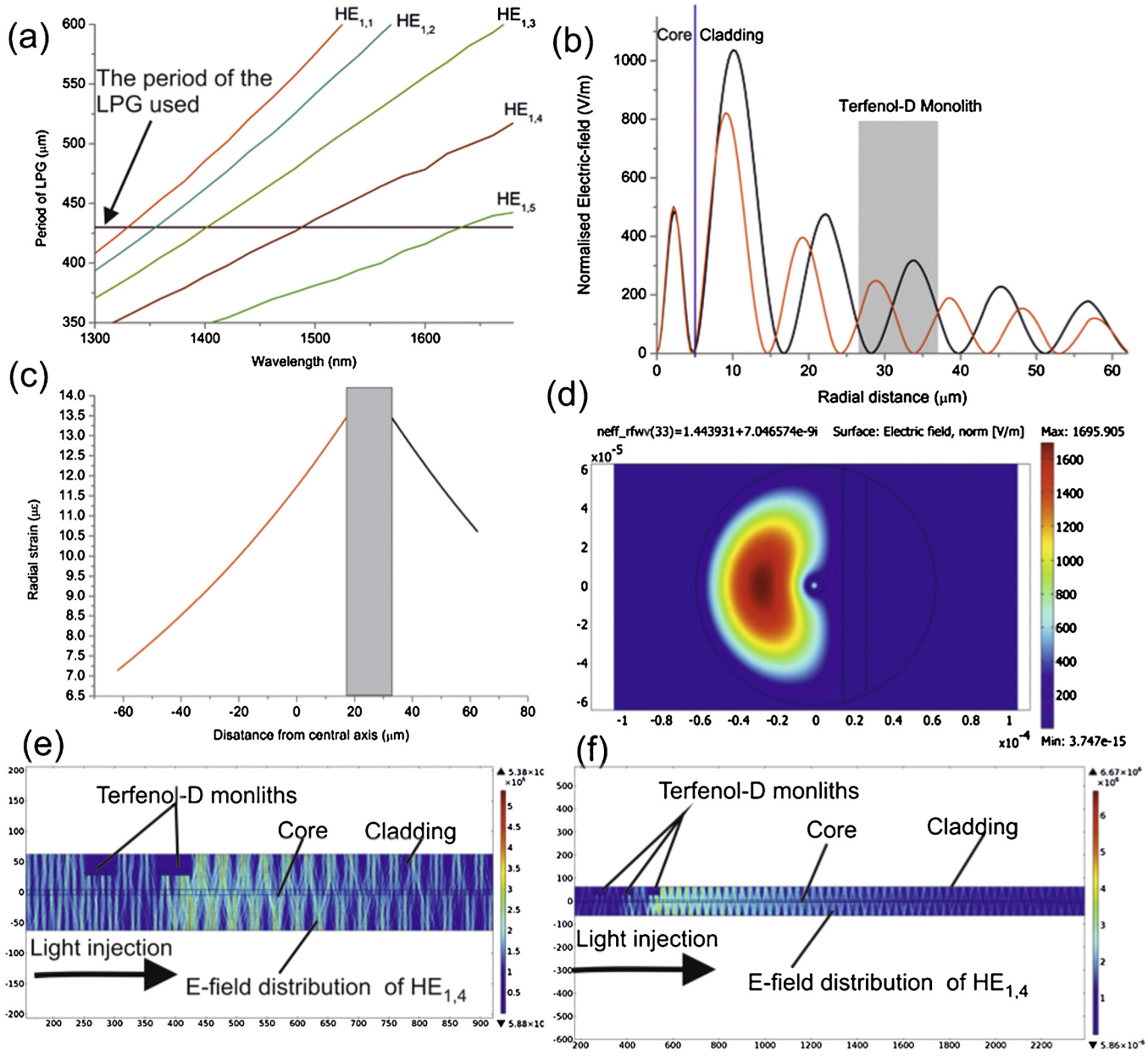


**Fig. 1.** (a) The phase-matching curves for a few of the attenuation bands for a long period grating with a period of 430 μm using SMF Telecoms optical fiber (b) The radial E-field distribution for the cladding modes $HE_{1,4}$ and $HE_{1,5}$ of the optical fiber and the position of the Terfenol-D monolith within the optical fiber (c) Shows the predicted radial strain induced by a Terfenol-D monolith in a static magnetic field with a magnitude of 1mT (d) Shows how the sculpted modified and coated optical fiber alters the radial E-field distribution for the $HE_{1,4}$ mode. (e) and (f) shows Finite Element Method model predicting the effect of the Terfenol-D monoliths on the E-fields of the cladding modes along the fiber for a two and three monolith device, respectively.

monoliths, $c$ is the velocity of light in vacuum. In this calculation $P$ is taken at fours angles, (parallel and perpendicular) to the magnetic field lines resulting from $p_{4,4}$ from the mechanical rotation of the fiber in the magnetic field. The authors do acknowledge the models used here to predict the spectral behavior of the new type of magnetic sensor are simplistic and that the strain created by the Terfenol-D monoliths will be a vector quantity, generating strains along the major three axes and additional shear strains.

Another factor that needs to be included is the overall effect of two or three monoliths on the entire LPG. This was analyzed by using the FEM package to simulate the electric field of the cladding modes in the z,y plane of travel for the experimentally investigated devices. Two monoliths perturb the E-field over a length of ~1.1 mm, whereas three monoliths produce a perturbed E-field over a length of 1.7 mm; Fig. 1e shows the perturbed E-field for the two cases. To better compare with experimental results, we estimate the net effect over the grating length by scaling the strain by the ratio of the total grating length to the sum of the lengths of the monoliths, this takes into the creation of longitudinal strain along the axis of the fiber, produced from the Terfenol-D monoliths. This leads to a reduction of 1/27 for the two-monolith device or 1/17 for that with three monoliths. Typical theoretical prediction results are shown in Fig. 2 for three monoliths. We note that any bending of the fiber in the presence of the B-field is excluded from the model. Inspecting the predictions shows that this device can produce a detectable wavelength shift for magnetic fields of moderate strength and has the ability to distinguish the direction of the field lines by producing either a red or blue wavelength shift, depending on the particular LPG attenuation band that is being assessed. It is expected that the induced bend generated by the

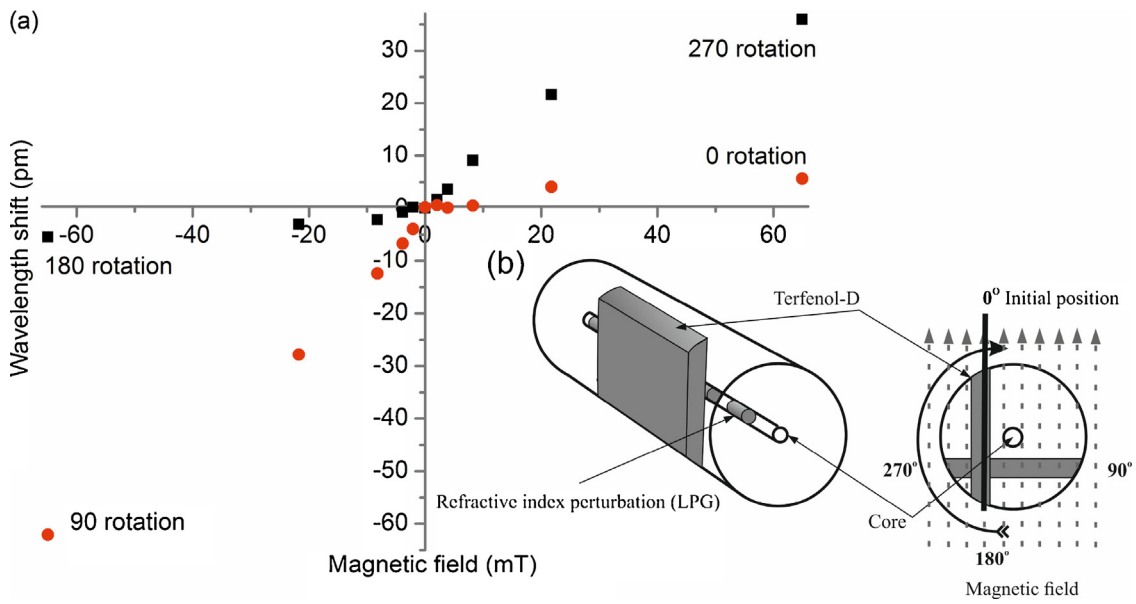


**Fig. 2.** (a) Theoretical prediction of the spectral sensitivity of single magnetostrictive fiber optic sensor to a static magnetic field consisting of three Terfenol-D monoliths running completely through the cladding (dimensions: length 50 μm, width 10 μm,) with spatial separations of 70 μm, with a radial displacement of 28 μm from the core/cladding interface, inscribed in the central region along the LPG length in the optical fiber. ■ and ● are labels for orthogonal data sets in the same quadrant. (b) Visualization of the orientation magnetic sensor and the illustration of the spatial orientations of the Terfenol-D monoliths in the optical fiber to the magnetic field lines.

monoliths of Terfenol-D would amplify the wavelength shift of the attenuation bands in addition to the strain-induced wavelength shift. This curvilinear waveguide can be visualised as an equivalent radially asymmetric index variation (using the conformal mapping technique [29]). This asymmetric index variation increases with increasing bend curvature of the optical fiber, these effective changes the index of the core and cladding modes to increase the refractive index differential and thus produce a wavelength shift which would be in addition to the stress/strain produced from the monoliths.

## 3. Fabrication of sensors

Based on our model, the parameters for the fabrication of the sensors were determined, and a three-stage, fabrication procedure was implemented. The first step involved the hydrogenation of standard single mode fiber (Corning SMF-28e) at a pressure of 200 bar, followed by the laser fabrication of a conventional LPG [22,23] (length of 30 mm, period 430 μm) into the fiber core, using a 244-nm UV laser (Coherent Sabre FreD); the average laser power was 100 mW. Following the LPG inscription, the fiber was annealed for 24 h at a temperature of 90 °C. Micro-slots were formed in the second step, using a femtosecond laser (Amplitude Systèmes s-Pulse HP femtosecond laser, operating at 1026 nm). The laser produces 500 fs laser pulses with a repetition rate of 1kHz, and the micro-slots were finished using the etching technique [20,30]. To reach the required power density, the laser pulses were focussed using a 100x objective lens (Mititoyo MPlan Apo NIR Series, numerical aperture 0.5) leading to a spot size on the sample of 1.5 μm, whilst using a pulse energy of 350 nJ [20,26]. Details of the procedure used for the aligning and the inscription of each micro-slot into the optical fiber are published elsewhere [13]. The device is subsequently submerged into a 5% hydrofluoric acid solution for chemical etching, which is placed in an ultrasonic bath for approximately 25 min to assist in the removal of the glass swarf; Fig. 3 c and d show the resultant sculpted fiber. The final step is to functionalize the sensor to a magnetic field; this is achieved by using the magnetostrictive material Terfenol-D. The microslots are “back filled” by using a RF sputtering machine, creating monoliths of Terfenol-D within the cladding of the fiber. As part of the process, a uniform coating of Terfenol-D was also applied along the length of the LPG with a coating thickness of 1 μm [3]. The resultant fiber devices have either two or three monoliths of Terfenol-D (length 50 μm, width 10 μm, depth ~100 μm) that go completely through the fiber's cladding, with each monolith separated by 70 μm and with a spatial offset of 28 μm from the core/cladding interface. They are located in the central section of the LPG.

## 4. Experimental characterization of the magnetic fiber sensor to static fields

Two permanent ferromagnets were used in the assessment of the magnetic sensors. Firstly, a ring magnet (pulling force of 6.4 kg) was used to examine the sensitivity of the magnetic fiber sensor to small magnetic fields (< 10 mT). Secondly, a horseshoe magnet (pulling force of 5.4 kg) was used to investigate two aspects of the sensors: the sensitivity of the sensor to much stronger magnetic fields (<60 mT) and to illustrate the potential of the fiber devices as vectorial sensors, measuring the magnetic field direction (Fig. 4 ). The spatial arrangement of apparatus for the first experiment is shown in Fig. 4b. The fiber sensor's monoliths were positioned along the central axis and at the midpoint within the ring magnet for the sensors to experience maximum field strength. Following this positioning the ring magnet was then translated along the length of the optical fiber away from the sensor, thus subjecting the sensor to a decreasing strength magnetic field. Because the sensor is anisotropic, the illuminating light used in the Characterization of the magnetic sensor was polarized to maximize the strength of the attenuation bands produced by the grating. The apparatus used for the illumination of the sensors, and the mechanical arrangements for the determination of the magnetic spectral sensitivities, is shown in Fig. 4. Typical transmission spectra are shown in Fig. 5 , it can be seen that an additional monolith (from two to three,) has reduced the optical strength of the resonances associated with the cladding modes $HE_{1,4}$ and $HE_{1,5}$ which is expected from the modelling, Fig. 5b.

The overall sensitivity of the sensors was investigated using the ring magnet; the results can be seen in Fig. 6 a and b for

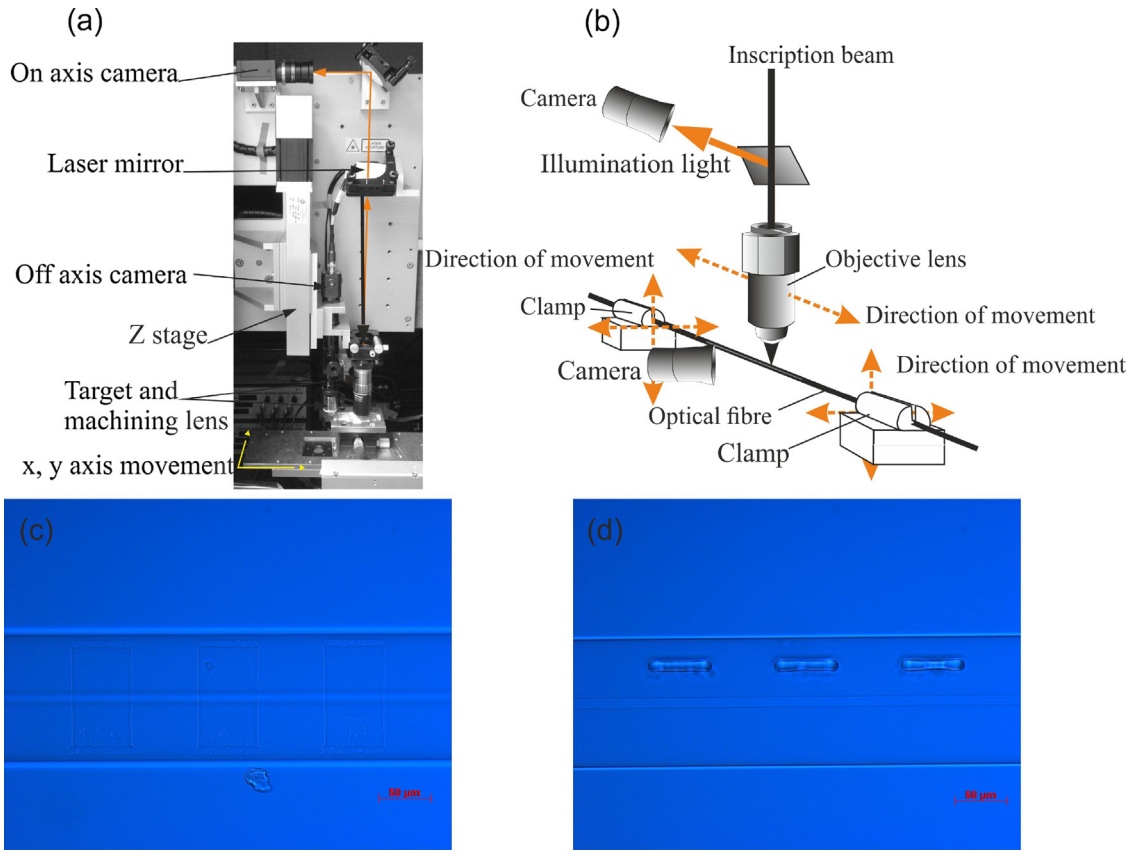


**Fig. 3.** (a) Picture of the opto-mechanical components of the femtosecond laser inscription scheme used to produce the slots in the optical fiber. (b) Schematic of the inscription set-up. The views of the finished sculpted LPG with slots: (c) the y-z plane; (d) the x-y plane (brightfield microscope images).

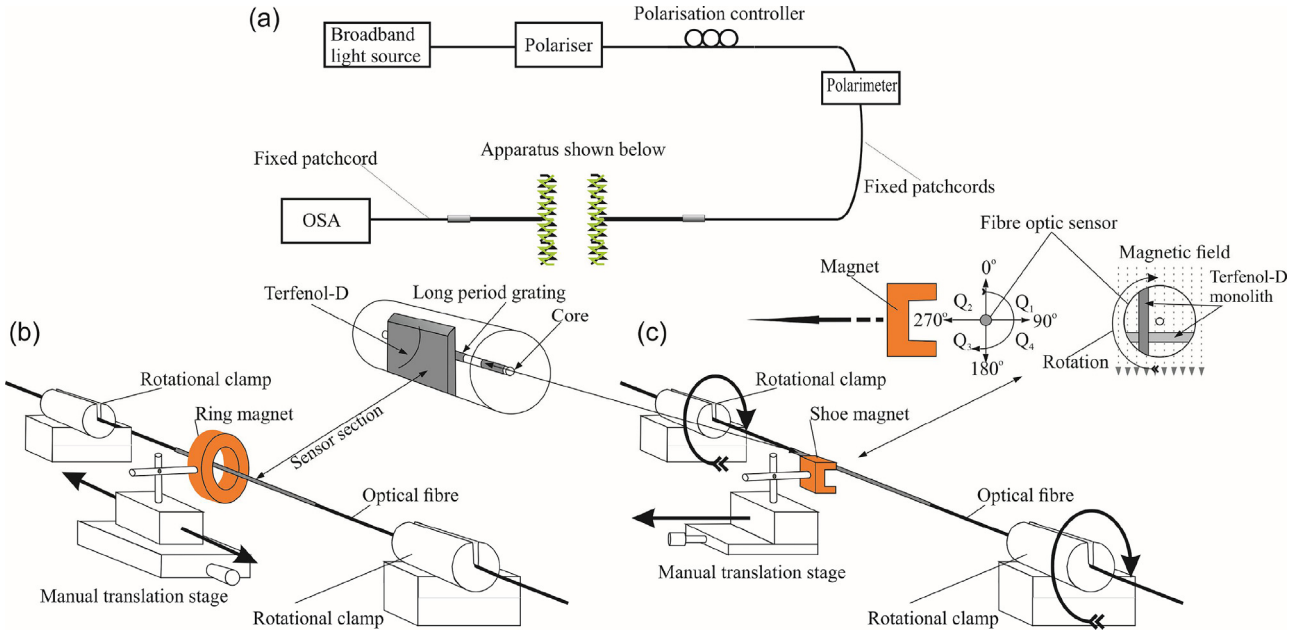


**Fig. 4.** The optical and mechanical apparatus used to investigate the magnetic spectral behavior and sensitivities of a single magnetostrictive fiber optic sensor. (a) The schematic of the apparatus used to illuminate and polarize the light and to identify the modifications in the spectral features in the transmission spectra when subjected to a magnetic field. (b) Mechanical arrangement used to determine the overall spectral sensitivities. (c) Mechanical arrangement used to investigate the dependency of spectral behavior on the orientation of the magnetic field.

two and three monolith optical fiber sensors, respectively, comparing the same attenuation bands at approximately the same spectral location. Fig. 6 suggests that the response of the 3 monolith sensor saturates at a lower field (4 mT) than the 2 monolith sensor (8 mT). The three monolith device yields a larger wavelength shift over the non-saturated condition of 93 pm compared to only

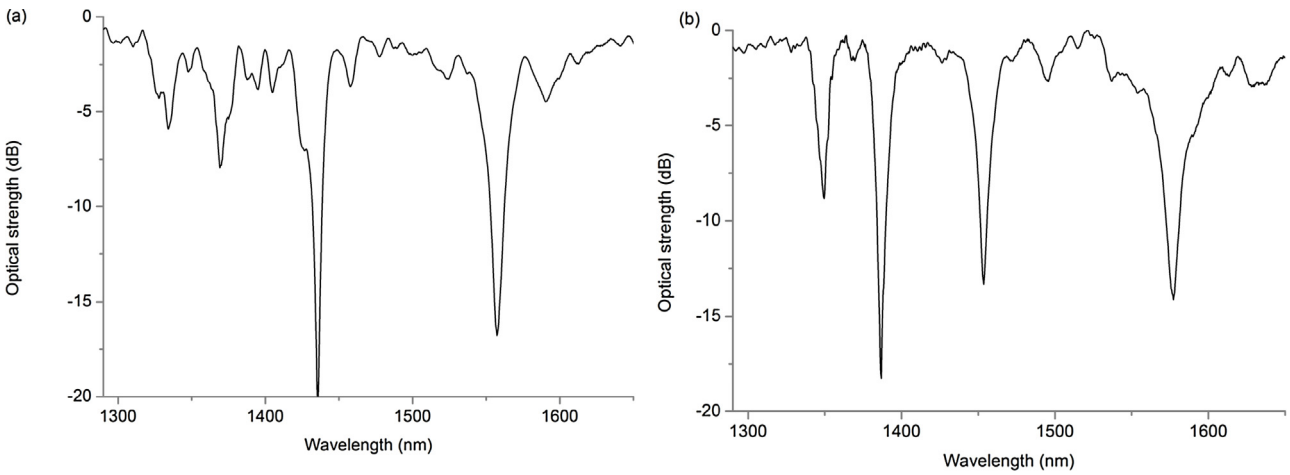


**Fig. 5.** Typical transmission spectra of the optical fiber magnetic sensors that have (a) Two Terfenol-D monoliths (b) Three Terfenol-D monoliths.

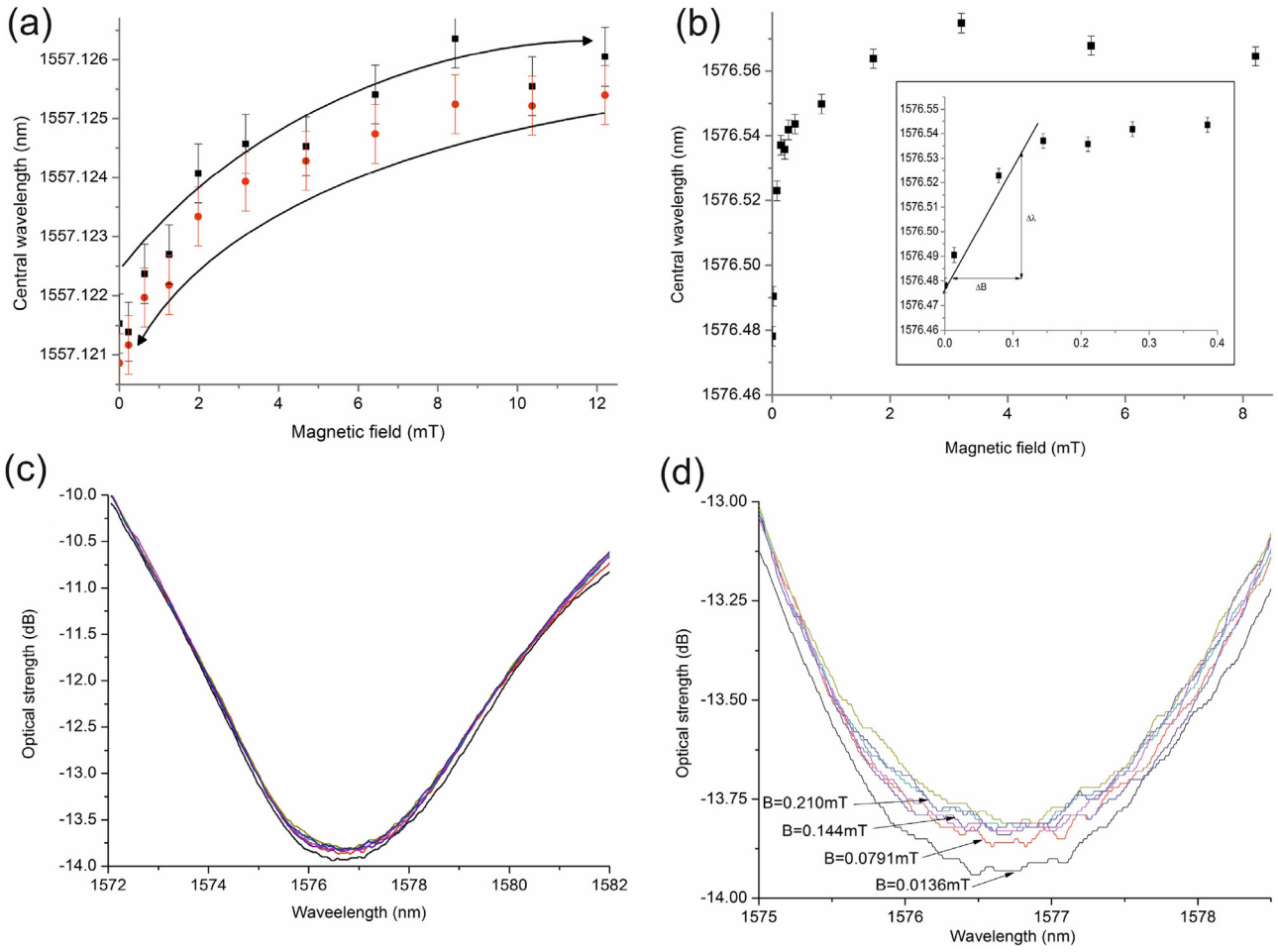


**Fig. 6.** Typical spectral sensitivities for magnetostrictive fiber optic magnetic sensors (a) Two Terfenol-D monoliths, showing the response to increasing (■) and decreasing (●) magnetic field strength. (b) Three Terfenol-D monoliths with an insert with an expanded scale of the lower magnetic field strengths applied. (c) and (d) typical changes in transmission spectra with an applied static magnetic field for a three monolith fiber device.

4 pm for the two monolith device. The sensors produced maximum spectral sensitivities of $\Delta\lambda/\Delta B = 5$ pm/mT over 0 to 8 mT (2 element device) and $\Delta\lambda/\Delta B = 543$ pm/mT over 0 to 0.4 mT (3 element device), the spectral sensitivity is a linear approximation over the first 4 measurements, insert in Fig. 6b. The three monolith sensor has approximately 18 pm/mT spectral sensitivity ranging up to a magnetic field strength of about 4 mT. A stability test was performed on the LPG's attenuation band strength and wavelength as determined from both the band minimum and using the centroid approach over 56 spectra taken over around 20 min at a constant temperature. This yielded a peak wavelength standard deviation of 0.05 nm and optical strength standard deviation of 0.05 dB along with a centroid wavelength standard deviation of 0.001 nm with a centroid optical strength standard deviation of 0.02 dB. Further-

more, inspecting Fig. 6c and d shows small and negligible changes in the optical strength of the attenuation band associated with the $HE_{1,5}$ cladding mode and there are no additional spectral features, such as a notch in the attenuation band, that would be associated with a grating phase change. These results have shown that changing the number of monoliths changes the effective operating regime with regards to the range of strength of magnetic field before device saturation occurs and are an indication that these devices can be tailored for a range of strengths of magnetic field. Furthermore, it is known that the magnetostrictive material Terfenol-D exhibits hysteresis, this was investigated for all sensors by observing the spectral responses of the sensors with increasing magnetic field strength to a maximum and then decreasing the magnetic field strength to zero, a typical example is shown in Fig. 6a. The spectral hysteresis of the sensors was limited and was of similar magnitude to the error within the experiments. These results appear to be consistent with results obtained with Terfenol-D monoliths in fiber working in conjunction with fiber Bragg gratings [3].

The directional dependency of the magnetic field sensitivity was investigated using the apparatus shown in Fig. 4c. The results for the three Terfenol-D monolith devices are shown in Fig. 7 . The sensitivities of the different attenuation bands are shown in Fig. 7a and b for attenuation bands associated with the $HE_{1,3}$ and $HE_{1,5}$ cladding modes, respectively. The different spectral behavior of the two bands is expected due to the differences in the radial distribution of the two cladding modes [25].

Differences in behavior were observed between the two sensors when subjected to changes in the applied magnetic field direction. The three Terfenol-D monolith sensor produced spectral sensitivities ranging from $\Delta\lambda/\Delta B = -8$ pm/mT to $-130$ pm/mT and $\Delta\lambda/\Delta B = +4$pm/mT to + 76 pm/mT for opposite orientations of the fiber within the magnetic field and negligible response for parallel orientations, please see Fig. 7b. The corresponding values for the two Terfenol-D monolith sensor were between $-2$ pm/mT and 1 pm/mT. Another experiment was performed to verify that polarization is the key mechanism responsible for the blue and red wavelength shifts with regards to magnetic fields that are opposite in directions. In this experiment, the sensing fiber remained static and the magnetic field was rotated through 180°; this revealed that the wavelength shifts are red shifted for both magnetic field line directions. These last two results confirm that the rotation of the fiber produces additional elliptical birefringence that enables information about the orientation of the sensor within the magnetic field and magnitude of that field.

## 5. Discussion

Comparing the theoretical predictions of Fig. 2 with the experimental results of Fig. 6b indicates a difference in spectral sensitivity and overall maximum wavelength shift. For example, the experimental spectral sensitivity at 90° for the 3 monolith is greater by a factor 3 than is predicted theoretically. There are several factors that could account for this difference. Firstly, the shear stresses produced by the Terfenol-D monoliths in a DC magnetic field may be more significant than initially considered and have greater effect on the elliptical birefringence generated by the rotation of the fiber.

Secondly, we have used a simple approximation that from the mechanical rotation $p_{4,4}$ is the only strain-optic coefficient responsible for the elliptical birefringence; the authors realize there will be other $p$ coefficients that will also contribute to the overall change in birefringence. Furthermore, the overall generation of birefringence due to strain from the Terfenol-D monoliths is simplistic; only accounting for radial and longitudinal strain, the authors acknowledge that the true strain is a vector quantity.

Thirdly, an additional wavelength shift of the attenuation bands may result from the sensor becoming curvilinear in shape under the influence of the magnetic field induced strain in the monoliths. The conformal mapping technique [28] says that a curved optical fiber waveguide having a curvature R can be replace with an equivalent straight waveguide with the following index profile $n(R) \rightarrow \left(n_0 + \frac{dn}{d\varepsilon} \cdot \varepsilon\right) exp\left(\frac{d}{R}\right)$. Where $n_0$ is the initial refractive index of the core/cladding, $R$ is the curvature experienced by the fiber and $d$ is the distance from the center of the fiber and $\varepsilon$ is the longitudinal strain created from the curvature. Thus, for very small displacements $d$, and using the expression for wavelength shift as a function of curvature Reference 23, leads to LPGs wavelength shift as proportional to $d/R^2$as a first approximation This is made complicated by the fact that sensor has been coated Terfenol-D, thus the cladding modes associated with the attenuation bands could be leaky or at least effected by the Terfenol-D material and therefore would change the overall sensitivity. Thus, these two factors can help to explain the larger wavelength shift observed experimental than predicted theoretically.

The sensor's resolution was determined using the method outlined in [31]. Considering the three monolith device, the full width half maximum of the attenuation band is 29.8 nm, using an optical spectrum analyzer provides 1000 discrete wavelength measurements, therefore $\Delta\lambda_{min}$ could in principle be 0.03 nm, however, this is beyond the resolution limits of the optical spectrum analyzer which has a minimum detectable wavelength change of $\Delta\lambda_{min} = 0.06$ nm. However, using the centroid approach yields a higher resolution of 0.01nm, leading to the following results. For $\Delta\lambda/\Delta B = 543$ pm/mT we obtain a static magnetic field resolution $\Delta\lambda_{min}$ $(\Delta B/\Delta\lambda)$ of $\pm 50$ μT for strengths below 0.4 mT and using a spectral sensitivity of 18 pm/mT gives a magnetic field strength resolution of $\pm 250$ μT over a range of a few mT, as shown in Fig. 6b.

The sensors' operating range (defined as the maximum magnetic field strength before saturation in wavelength shift occurs) depends upon on the number of Tefenol-D monoliths. The directional magnetic field experimental data in Fig. 7b, when compared with the results obtained from the ring-magnet (Fig. 5b for 0° and 180° orientations) indicate saturation at ∼ 5 mT, which is similar to the previous results shown in Fig. 6b. The attenuation band associated with the $HE_{1,3}$ cladding mode shows that the saturation condition occurs at a higher magnetic field strength of ∼ 8 mT. Furthermore, the $HE_{1,5}$ cladding mode yields higher sensitivities, larger wavelength shifts and saturation levels occurring at higher magnetic field strengths of $-40$ mT and + 20 mT, compared to the attenuation band associated with the $HE_{1,3}$ cladding mode at the 90° and 270° orientations. Another observation is that there is some asymmetric spectral response, between 90° and 270° orientation (perpendicular to the magnetic fields line) yielding different maximum wavelength shifts, which is seem in the theoretical predictions. This is the result of the birefringence induced from the mechanical rotation of the fiber adding to the overall spectral sensitivity and the maximum wavelength shift produced by the stress induced from the Terfenol-D monoliths in one rotation direction, i.e. 90° and when the fiber is rotated in opposite direction to 270° this is subtractive to the birefringence stress induced by the Terfenol-D monoliths. Also, this spectral behavior may suggest that the monolith slots are not parallel to the central axis of the fiber, having a slight angle of incline.

Saturation at these low field values could be considered unusual behavior just considering the magnetostrictive properties of the Terfenol-D material, which has a saturation magnetic field strength of 1 T [32]. The monoliths are situated within another material that is effectively pure amorphous silica then this saturation may be expected. The Terfenol-D changes shape in the presence of a magnetic field, thus generating a force against the medium that

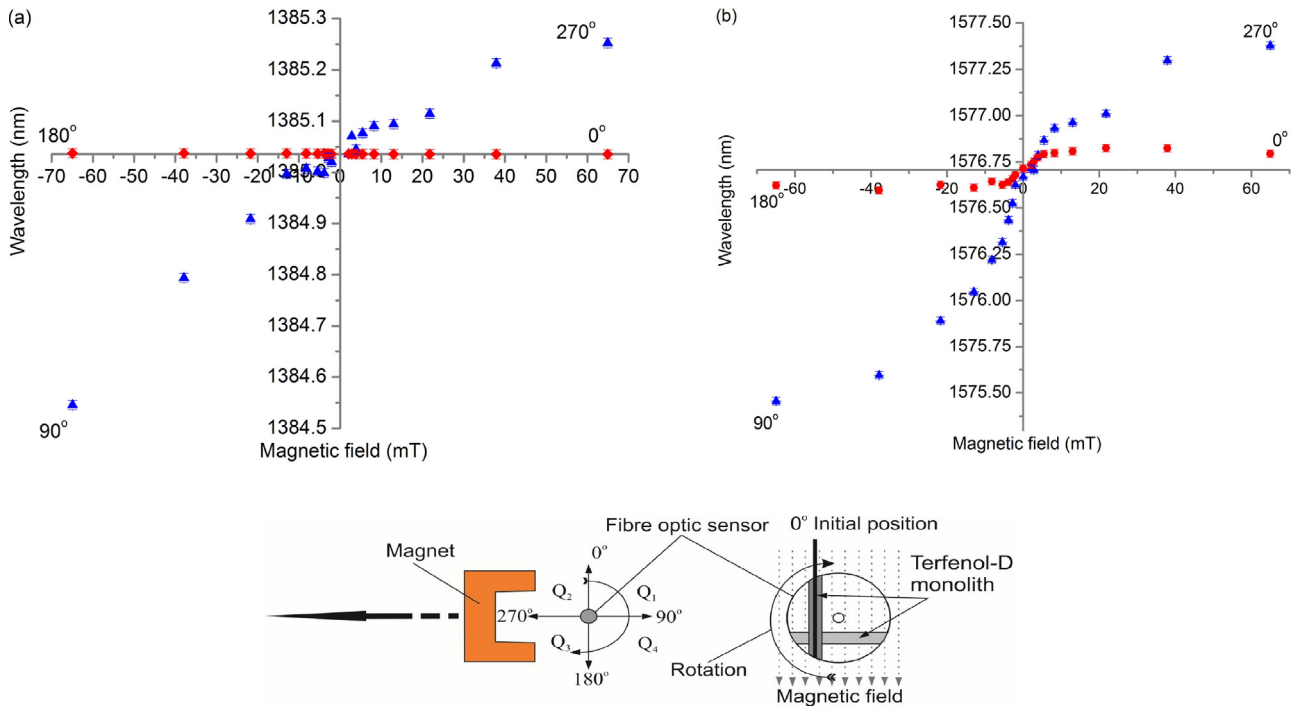


**Fig. 7.** The spectral response of different attenuation bands of the three Terfenol-D monoliths device. (a) and (b): attenuation bands associated with the $HE_{1,3}$ and $HE_{1,5}$ cladding modes, at 1385 nm and 1576.75 nm respectively. (c)Visualization of the spatial orientation of the sensor to magnetic field lines.

surrounds the monoliths, the stress field in the medium in turn provides mechanical resistance to the change in shape of the monolith (and changes in birefringence). With the ring magnet, the magnetic field lines are along the central axis of the fiber (with a large bulk of material), thus as the monolith changes shape it experiences mechanical resistance from the optical fiber. Furthermore, this net mechanical resistance to movement, produced in the silica cladding region, would be reached for a lower DC magnetic field if there were more monoliths present in the fiber device. This is observed experimentally; there is higher spectral saturation response for the device with two monoliths compared to the three monolith device, 10 mT and 2 mT, respectively.

Using the same argument with the horseshoe magnet, the magnetic field lines are perpendicular to the optical fiber central axis and thus there is less bulk silica to offer mechanical resistance so the saturation occurs with a higher magnetic field strength, which again is observed experimentally. Furthermore, with the horseshoe magnet the Terfenol-D monolith produces a curve along the fiber and thus create additional wavelength change in the attenuation bands of the LPG that wouldn't be seen with the ring magnet.

Other possible additional effects that can produce further wavelength shifts are the changes in the effective refractive index of the monolith itself under the influence of a DC magnetic field, along with additional shear strains at the cladding-monolith interface. This effect would be small with insignificant change to the coupling coefficients and efficiency resulting in a negligible change in the optical strength of the attenuation band.

We have stated that the fiber asymmetry and its mechanical rotation are responsible for any red and blue wavelength shifts in the presence of the magnetic field. As the fiber is rotated to a new relative orientation (0°, 90°, 180° and 270°), there will be a section of fiber with elliptical birefringence [24,27,28] that the illuminating light will pass through. Prior to any measurement at a new rotation angle, the polarization controller is used to reset the LPG's resonance wavelength to its original spectral value. Secondary to this elliptical birefringence the asymmetric geometry produced by the Terfenol-D monoliths within the cladding, gives rise to an azimuthal polarization dependency. Examples of typical azimuthal polarization dependencies of the attenuation bands of the devices with no applied magnetic field are shown in Fig. 8 a and b. The results shown are associated with the attenuation bands used in Fig. 5a and b and show wavelength dependences of 7 pm/degree and 17 pm/degree for the two and three monolith devices, respectively, with the same optical strength variation of 0.05 dB/degree. The degree of azimuthal polarization sensitivity is dependent upon which cladding mode, and its associated attenuation band, is being monitored. The different attenuation bands displayed polarization sensitivities varying from 4 pm/degree to 42 pm/degree with greater sensitivities produced at longer wavelengths and an average polarization value of 7 pm/degree.

The temperature sensitivity of the attenuation bands used for the magnetic measurements was also investigated, yielding values of 18 pm/°C and 26 pm/°C for the two and three Terfenol-D monolith sensors, respectively. The wavelength cross-talk between the static magnetic field strength and ambient temperature was estimated using experimental data and other material properties from reference [24], Table 1.

A Taylor expansion of the phase matching condition $\lambda = \delta n \Lambda$ leads to

$$\Delta\lambda_{Tot} = \delta n + \frac{\partial\lambda}{\partial B}\Delta B + \frac{\partial\lambda}{\partial T}\Delta T + \frac{\partial^2\lambda}{\partial B\,\partial T}\Delta T\Delta B$$

Writing $\frac{\partial\lambda}{\partial B}\Delta B = \frac{\partial\lambda}{\partial B}\frac{\partial B}{\partial\varepsilon}\Delta\varepsilon = \left[\frac{\partial\lambda}{\partial\varepsilon}\right]_{\lambda}\frac{\partial\varepsilon}{\partial B}\Delta B$

and using $\frac{\partial\lambda}{\partial\varepsilon} = \frac{\partial\lambda}{\partial B}\frac{\partial B}{\partial\varepsilon}$

leads to $\frac{\partial^2\lambda}{\partial B\partial T}\Delta T\Delta B = \Delta T\Delta B\left\{\left(\Lambda\left[\frac{\partial\delta n}{\partial\lambda}\frac{\partial\lambda}{\partial B}\right] + \delta n\left[\frac{\partial\Lambda}{\partial\varepsilon}\frac{\partial\varepsilon}{\partial B}\right]\right)\frac{\partial\lambda}{\partial T}\right\}$

where we have assumed that the increase in the period of the LPG is linearly proportional to strain, thus $\frac{\partial\Lambda}{\partial\varepsilon} = 1$. This yields an insignificant value of approximately $1.6 \times 10^{-2}$ pm°C$^{-1}$ mT$^{-1}$. This cross-sensitivity result and the experimentally determined low temperature spectral sensitivities show that it would be feasible to operate the device in an uncontrolled environment, so long as the temperature of the device were measured with an accuracy

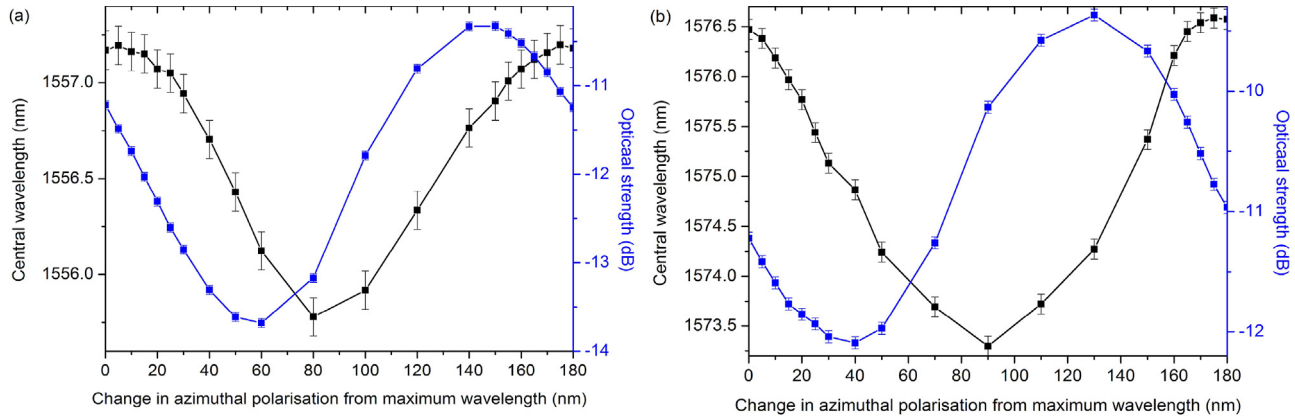


**Fig. 8.** Examples of the LPGs attenuation bands wavelength and optical strength dependence upon azimuthal polarization with no applied magnetic field from the maximum wavelength (a) a two monolith (b) a three monolith fiber device.

**Table 1**
Optical constants.

| Layer | Refractive | Thermal Expansion | Strain-optic | Thermo-optic | Radius | Material |
|---|---|---|---|---|---|---|
| core | $n_1 = 1.458$ | $4.1 \times 10^{-7}$ | 0.28 | $7.3 \times 10^{-6}$ | $3.8 \times 10^{-6}$ | $GeO_2$/B / $SiO_2$ |
| cladding | $n_2 = 1.4446$ | $4.1 \times 10^{-7}$ | 0.24 | $7.8 \times 10^{-6}$ | $62.5 \times 10^{-6}$ | $SiO_2$ |

around 0.1. This could be readily achieved suing a collocated FBG, for example.

It is informative to compare the results of this paper with those of other researchers investigating optical fiber magnetic sensors using fiber Bragg grating technology [3,13,14]. Typical values for sensitivity range from 0.5 pm/mT to 1 pm/mT, which are approximately 2 orders of magnitude smaller than ours. Typical resolutions are ±300 μT [3], which is 6 times poorer than we are reporting here. There are magnetostrictive fiber optic sensors/array that have been used to yield orientation and magnitude of magnetic fields [16,17] the exhibit low sensitivities of 1.2 pm/mT and 2.5 pm/mT with typical detection limits ranging from 0.3 to 0.4 mT [16,17] which are 2 orders of magnitude smaller than ours and their resolution is poor compared to the presented sensor in this paper.

Other optical fiber magnetic sensors using magnetic fluids and photonic crystal fibers (PCF) yield lower sensitivity values, for example 29 pm/mT to 45 pm/mT [33–35]. These sensors based upon magnetic fields have issues detecting low strength magnetic fields with typical detection limits of 2 mT [18,19,27]. There are other examples of fiber sensors that use tapers [11]; again, the overall sensitivity is lower compared to the sensor presented in this paper. Yet another sensor using the Verdet effect [36] yields high sensitivity (with a resolution of 2 μT) but only at high magnetic field strengths. More recently researchers have used a plasmonic device with a tilted fiber Bragg grating and a magnetic fluid 19] that yields good spectral sensitivity but appears to be usable from around 2 mT and higher. The researchers show orientation wavelength shift dependence; it is well known that plasmons and tilted Bragg gratings are highly sensitive to the polarization of the light but the researchers didn't present the polarization dependence, which may have a major effect on the performance of the plasmonic device.

The time response of our devices has not been investigated due to the fact that an optical spectrum analyzer has been used to interrogate the devices, which would be the limiting factor at present; thus, we are only considering DC magnetic fields in this study.

The main advantage with this sensor is a significant increase in sensitivity of approximately 2 orders of magnitude over other similar fiber optic magnetic field strength sensors. This device yields a typical spectral sensitivity of $\Delta\lambda/\Delta B = 540$ pm/mT in low static magnetic field values up to 4 mT with a resolution of ±50 μT for field strengths of sub-mT. Moreover, the sensing device presented has an overall detection limit that is approximately one order of magnitude smaller than the best previously reported fiber optical DC magnetic sensing devices. Furthermore, whilst the sensor is not a vectorial magnetic field sensor it can yield information on the sensor's orientation within a static magnetic field.

The reported performance values are approaching the requirements for determining the earth's magnetic field (25–65 μT) [7], suggesting that once optimized this approach has potential applications in geophysical activities, which to date have not been possible with these types of magnetic sensors.

## Author contributions

The contribution of the authors is as follows: T. A., K.K. and G.L. developed the original sensing concept. T.A., G.L., K.K., D.J.W. designed, modelled, designed experiments, analyzed the data for the magnetic sensing devices. T.A., G. L., C. W., R.N., fabricated the sensors. T. A., G. L. performed characterization experiments. The manuscript was written by T.A., R. N., C. W., G. L., K.K., D.J.W. and P.C. All authors engaged in discussions with regards to the results obtained and all commented on the manuscript.

## Acknowledgment

This work was financially supported by grants EP/J010413 and EP/J010391 for Aston University and the University of Plymouth from the UK Engineering and Physical Sciences Research Council.

## References

[1] P. Stavroulakis, Biological Effects of Electromagnetic Fields, Springer, New York, 2003.
[2] Z. Sienkiewicz, Biological effects of electromagnetic fields, Eng. Sci. Educ. J. 7 (3) (1998) 127–134.
[3] G.N. Smith, T. Allsop, K. Kalli, C. Koutsides, et al., Characterization and performance of a Terfenol-D coated femtosecond laser inscribed optical fiber

bragg sensor with a laser ablated microslot for the detection of static magnetic fields, Opt. Exp. 19 (1) (2011) 363–370.
[4] S.-C. Yan, Y. Chen, C. Li, F. Xu, Y.-Q. Lu, Differential twin receiving fiber-optic magnetic field and electric current sensor utilizing a microfiber coupler, Opt. Exp. 23 (7) (2015) 9408–9411.
[5] M.F. Rahman, L. Zhong, Md.E. Haque, M.A. Rahman, A direct torque-controlled interior permanent-magnet synchronous motor drive without a speed sensor, IEEE Trans. Energy Convers. 18 (1) (2003) 17–22.
[6] F. Gueissaz, D. Piguet, The MicroReed, an ultra-small passive MEMS magnetic proximity sensor designed for portable applications, MEMS 2001, in: 14th IEEE International Conference on Micro Electro Mechanical Systems, 2001, pp. 269–273.
[7] A. Almasil, A. Jafarirad, P. Afzal, M. Rahimi, Orogenic gold prospectivity mapping using geospatial data integration, region of Saqez, NW Iran, Bull. Miner. Res. Explor. 150 (2015) 65–76.
[8] S. Yu, R. Tang, Electromagnetic and mechanical characterizations of noise and vibration in permanent magnet synchronous machines, IEEE Trans. Magn. 42 (4) (2006) 1335–1338.
[9] G. Zhao, J. Hu, Y. Ouyang, W. Chang, Z. Wang, S.X. Wang, J. He, J. Bi, Novel method for magnetic field vector measurement based on dual-axial tunneling magnetoresistive sensors, IEEE Trans. Magn. 53 (8) (2017) 4400306.
[10] Y. Sugita, H. Fujiwara, T. Sato, Critical thickness and perpendicular anisotropy of evaporated permalloy films with stripe domains, Appl. Phys. Lett. 10 (1967) 229–231.
[11] A. García-Arribas, J. Gutiérrez, G.V. Kurlyandskaya, J.M. Barandiarán, et al., Sensor applications of soft magnetic materials based on magneto-impedance, magneto-elastic resonance and magneto-electricity, Sensors 14 (5) (2014) 7602–7624.
[12] L. Jogschies, D. Klaas, R. Kruppe, J. Rittinger, et al., Recent developments of magnetoresistive sensors for industrial applications, Sensors 15 (11) (2015) 28665–28689.
[13] Y.-T. Dai, M. Yang, J.M. Karanja, Q. Zhao, Novel FBG sensors based on cladding surface microstructures, Santander, Spain, 9157, SPIE Proc., 23rd International Conference on Optical Fiber Sensors (2014), 91570J-1.
[14] M. Yang, J. Dai, C. Zhou, D. Jiang, Optical fiber magnetic field sensors with TbDyFe magnetostrictive thin films as sensing materials, Opt. Exp. 23 (17) (2009) 20777–20782.
[15] F.T. Calkins, A.B. Flatau, M.J. Dapino, Overview of magnetostrictive Sensor Technology, J. Intell. Mater. Syst. Struct. 18 (2007) 1057–1066.
[16] H. García-Miquel, D. Barrera, R. Amat, G.V. Kurlyandskaya, S. Sales, Magnetic actuator based on giant magnetostrictive material Terfenol-D with strain and temperature monitoring using FBG optical sensor, Measurement 80 (2016) 201–206.
[17] S.M.M. Quintero, A.M.B. Braga, H.I. Weber, et al., A magnetostrictive composite-fiber Bragg grating sensor, Sensors 10 (9) (2010) 8119–8128.
[18] J. Yin, P. Yan, H. Chen, Li Yu, J. Jiang, M. Zhang, S. Ruan, All-fiber-optic vector magnetometer based on anisotropic magnetism-manipulation of ferromagnetism nanoparticles, Appl. Phys. Lett. 110 (23) (2017) 231104.
[19] Z. Zhang, T. Guo, X. Zhang, J. Xu, W. Xie, M. Nie, Q. Wu, B.-O. Guan, Jacques Albert, Plasmonic fiber-optic vector magnetometer, Appl. Phys. Lett. 108 (10) (2016) 101105.
[20] G.C.B. Lee, C. Mou, K. Zhou, K. Sugden, Optimization and characterization of femtosecond laser inscribed in-fiber microchannels for liquid sensing, Santander, Spain, 9157, SPIE Proc., 23rd International Conference on Optical Fiber Sensors (2014) 915743–915747.
[21] R.M. Silva, H. Martins, I. Nascimento, J.M. Baptista, et al., Optical current sensors for high power systems: a review, Appl. Sci. 2 (3) (2012) 602–628.
[22] K.O. Hill, G. Meltz, Fiber bragg grating technology and overview, J. Lightwave Technol. 15 (8) (1997) 1263–1276.
[23] T. Allsop, A. Gillooly, V. Mezentsev, T. Earthgrowl-Gould, et al., Bending and orientational characteristics of long period gratings written in D-shaped optical fiber, IEEE Trans. Instrum. Meas. 53 (1) (2004) 130–135.
[24] T. Allsop, D.J. Webb, I. Bennion, A comparison of the sensing characteristics of long period gratings written in three different types of fiber, Opt. Fiber Technol. 9 (4) (2003) 210–223.
[25] G.C.B. Lee, C. Mou, K. Zhou, K. Sugden, Optimization and characterization of femtosecond laser inscribed in-fiber microchannels for liquid sensing, J. Lightwave Technol. 33 (12) (2015) 2561–2565.
[26] A. Bertholds, R. Dandliker, Determination of the individual strain-optic coefficients in single-mode optical fibers, J. Lightwave Technol. 6 (1) (1988) 17–20.
[27] Y.P. Wang, Y.J. Rao, Long period fiber grating torsion sensor measuring twist rate and determining twist direction simultaneously, Electron. Lett. 40 (3) (2004) 164–166.
[28] K. Okamoto, T. Edahiro, N. Shibata, Polarization properties of single-polarization fibers, Opt. Lett. 7 (11) (1982) 569–571.
[29] M. Heiblum, J. Harris, Analysis of curved optical waveguides by conformal transformation, IEEE J. Quant. Electron. 11 (2) (1975) 75–83.
[30] Y. Lai, K. Zhou, L. Zhang, I. Bennion, Microchannels in conventional single-mode fibers, Opt. Lett. 31 (17) (2006) 2559–2561.
[31] J. Hu, X. Sun, A. Agarwal, L.C. Kimerling, Design guidelines for optical resonator biochemical sensors, JOSA B 26 (5) (2009) 1032–1041.
[32] ETREMA Products Inc. http://www.etrema.com/terfenol-d/ (2015).
[33] H. Chen, S. Li, J. Li, Z. Fan, Magnetic field sensor based on magnetic fluid selectively infilling photonic crystal fibers, IEEE Photonics Technol. Lett. 27 (7) (2015) 717–720.
[34] P. Zu, C.C. Chan, W.S. Lew, Y. Jin, et al., Magneto-optical fiber sensor based on magnetic fluid, Opt. Lett. 37 (3) (2012) 398–400.
[35] Y. Zheng, X. Dong, C.C. Chan, P.P. Shum, H. Su, Optical fiber magnetic field sensor based on magnetic fluid and microfiber mode interferometer, Opt. Commun. 336 (2015) 5–8.
[36] L. Sun, S. Jiang, J.R. Marciante, All-fiber optical magnetic-field sensor based on Faraday rotation in highly terbium-doped fiber, Opt. Exp. 18 (6) (2010) 5407–5412.

## Biographies

**Thomas D. P. Allsop** received the B.Sc. (honors) degree in physics and astrophysics from Queen Mary College, University of London, London, U.K., the M.Sc. degree in opto-electronics from the University of Northumbria, Newcastle, U.K., and the Ph.D. degree in photonics from the University of Plymouth, Plymouth, U.K., in 1985, 1992, and 1998, respectively. He has been a Senior Research Fellow with the Aston Institute of Photonic Technologies, Aston University, Birmingham, U.K., since 2010. Prior to the current situation, he was worked on short-term contracts as an Optical Engineer in 2010 and for a short time on a LASERLAB EUROPE project (cooling of Yb atoms in a magneto optical trap this experiment) with the European Laboratory for Non-Linear Spectroscopy, University of Florence, Firenze, Italy, in 2010. Previously, he was a Senior Research Fellow with the Photonics Research Group, Aston University, for nearly 12 years. He has more than 80 journal and conference publications with over 70 publications as first author, along with being a named inventor on 11 international patents. His current research interests include fiber optical/plasmonic sensors with particular interest in chemical/biological/medical sensing applications, with a growing activity and interest in femtosecond laser interaction with materials.

**Graham B. Lee** received the Ph.D. and BEng degree from the University of Aston, Birmingham, U.K., in 2014 and 2009, respectively. After graduating, he had worked as a Research Fellow at the Aston Institute of Photonic Technologies, Birmingham from 2014 to 2015. Since 2016, he has worked as a Networks Design Engineer at Jaguar Land Rover and also a visiting research fellow at Aston University. His research interests include femtosecond laser micromachining and inscription, optical fiber sensors and optical sensors interrogation technologies.

**Changle Wang** received the B.S. and M.S. degrees in physics from Tianjin University, Tianjin, China, in 2009 and 2012, respectively. He is currently working toward the Ph.D. degree from Aston University, Birmingham, U.K. His research interests include advanced fiber grating devices in multicore fibers and multimode fibers, and their applications in optical fiber communication systems and fiber sensing.

**Ronald Neal** was spent in industry, engaged in researching and developing detectors and instrumentation for hydrocarbon gas analysis and nuclear radiation. He moved into microwave generation and amplification. He entered academia, lecturing on material science, laser technology, and optical communication. He is a Chartered Engineer with the Institution of Engineering and Technology, Stevenage, Herts, U.K. He is co-author of 25 journal and conference papers. He holds three joint patents for this research work. His current research interests include thin film materials deposition, optical fiber sensors, and surface plasmon resonance.

**Kyriacos Kalli** (M'00) received the B.Sc. (honors) degree in theoretical physics and the Ph.D. degree in physics from the University of Kent, Canterbury, U.K., in 1988 and 1992, respectively, where he studied linear and non-linear phenomena in optical fibers. He was a Visiting Research Scholar with Virginia Polytechnic Institute and State University, Blacksburg, in 1993, where he studied optical fiber sensors. From 1994 to 1996, he lectured and undertook research with the University of Kent into the use of fiber Bragg gratings in multiplexed sensor arrays and Raman spectroscopy. At the University of Cyprus, Nicosia, Cyprus, where he was engaged in research into integrated gas flow and gas sensors based on porous silicon micromachining, fluorescence spectroscopy, and nondestructive evaluation of semi-conductors. Since 2001, he has been a Lecturer with Higher Technical Institute, Nicosia, where he created and headed the Nanophotonics Research Laboratory. From 2008 he has been at Cyprus University of Technology as an Assistant Professor with the Department of Electrical Engineering/Computer Engineering and Informatics. He has more than 150 journal and conference publications. He has co-authored fiber Bragg gratings, Fundamentals and Applications in Telecommunications and Sensing (Norwell MA: Artech House, 1999), and has several other book contributions. His current research interests include Bragg grating and optical fiber sensors, photonic switching devices, multiplexing of optical sensors, and laser material interactions. Dr. Kalli is a member of the Institute of Physics and the Optical Society of America.

**Philip Culverhouse** (M'84) is an Associate Professor of computer vision and engineering design. He has been a Principal Investigator on four EU RTD contracts since 1992. The most recent completed August 2005 and delivered three underwater phytoplankton-monitoring instruments to partners in Spain, Italy, and Ireland. The machines use advanced vision pattern analysis and machine learning to recognize taxa and species of harmful algae, for early warning to fisheries aquaculture sites. He has more than 80 academic publications including over 40 on natural object recognition. He is the Co-Chair of the International Working Group 130 on automatic plankton identification sponsored by the Scientific Committee on Oceanic Research and the Royal Society, U.K. He leads the Bunny Robot Project, a low power multi-processor humanoid bipedal robot (Wolf et al., 2009) where he is responsible for a number of student-led robot visual guidance and object identification projects (Culverhouse et al., 2009). He has also led a number of KTP programs in control engi-

neering and engineering design Culverhouse operates within the newly founded Centre for Robotics and Neural which has the aim to foster world-leading interdisciplinary research in the field of neural and cognitive systems and their applications to robots and interactive intelligent systems.

**David J. Webb** received the B.A. degree in physics from the University of Oxford, Oxford, U.K., and the Ph.D. degree in physics from the University of Kent, Canterbury, U.K., in 1983 and 1989, respectively. He has worked at Aston University ever since 2001 and now is a Professor with the Aston Institute of Photonic Technologies, Aston University, Birmingham, U.K. Previously he had spent ten years with the University of Kent and was also with Oxford University, Oxford, and GEC Research, London, U.K. He has published work on stimulated Brillouin scattering and photorefractive non-linear optics. He has published over 300 journal and conference papers on these subjects. His current research interests include optical fiber sensing using in-fiber Bragg gratings and fiber interferometers, medical and biochemical applications of optical sensing technology, and development of polymer optical fiber based grating devices.